AIAA JOURNAL
Vol. 39, No. 5, May 2001

Dynamic Calibration of a Shear-Stress Sensor Using Stokes-Layer Excitation

Mark Sheplak,* Aravind Padmanabhan,† Martin A. Schmidt,‡ and Kenneth S. Breuer§
Massachusetts Institute of Technology, Cambridge, Massachusetts 02139

The design and implementation of a novel dynamic calibration technique for shear-stress sensors is presented. This technique uses the oscillating wall shear stress generated by a traveling acoustic wave as a known input to the shear-stress sensor. A silicon-micromachined, floating-element shear-stress sensor has been dynamically calibrated up to 4 kHz using this method. These data represent the first broadband, experimental verification of the dynamic response of a shear-stress sensor.

Introduction

THE measurement of shear-stress fluctuations in a turbulent boundary layer is of vital importance to the fluid mechanics community because it provides important information about flow phenomena, including viscous drag, transition to turbulence, and flow separation.[1] To capture accurately the spectrum of the turbulent shear-stress fluctuations, the measurement device must possess a large usable bandwidth, and the spatial dimensions of the device must be smaller than the turbulent structures to be measured. The spatial length scales of interest are typically on the order of 100 μm, and the required bandwidth is in excess of 10 kHz (Ref. 2). The stringent spatial and temporal resolution requirements naturally point to a microfabricated transducer as a means of achieving this level of performance, and a number of researchers have demonstrated device designs aimed at meeting this goal.[3–21] Existing wall shear-stress sensors can be grouped by measurement method into two distinct classes: direct techniques such as floating element type devices[3–11] or indirect techniques such as hot films[5,12–20] or hot wires.[21]

For turbulence measurements it is desirable that the shear-stress sensor possesses an optimally flat, unity-gain, minimum-phase frequency response function. Such characteristics are necessary to minimize the uncertainty in correlation and spectral analysis data. The actual dynamic response, however, will be band-limited because of the inherent compliance, inertance, and dissipation in the measurement system. For direct measurement techniques either the fluidic damping or the resonant frequency associated with the floating element structure defines the usable bandwidth. In thermal systems, the bandwidth is usually limited by the thermal inertia of the sensing element. In addition, the dynamic response of thermal sensors is complicated by the frequency-dependent heat conduction into the supporting structure (i.e., substrate[12,16–18,22,23] or membrane[13–15,19,20] for hot films and prongs for hot wires[21,24]), which creates a low-frequency roll off in the gain factor of the frequency response function, as well as a corresponding frequency-dependent phase lag. The difficulties associated with the modeling of time-resolved microscale phenomena, fluidic damping for floating elements and the conjugated heat-transfer problem for thermal sensors, precludes the accurate prediction of the frequency response function for both classes of shear-stress sensors. Therefore, it is necessary to characterize the frequency response function of the sensor via in situ dynamic calibration. Unfortunately, obtaining a known broadband shear-stress input for direct dynamic calibration is difficult in practice. Recently, a technique has been reported that calibrates shear-stress sensors using acoustically generated Stokes waves at various frequencies within a flat-plate boundary layer (M. N. Glauser, private communication, Arizona State University's Sensor Fest'97, 1998). The Stokes wave is generated in the wind-tunnel test section at a given frequency within a predetermined range via an array of nine speakers. The shear stress on the surface is calculated using a hot-wire velocity measurement at the same streamwise location as the surface-mounted sensor. This method has been used over a frequency range from 50 Hz to 3.0 kHz. This technique is very useful for absolute calibrations, but it requires a dedicated wind-tunnel facility outfitted with a speaker array and is ultimately band-limited as a result of spatial measurement resolution within the Stokes-layer velocity profile [i.e., $\delta(f) \approx 6.5\sqrt{(\nu/2\pi f)}$, $\delta(3\text{ kHz}) \approx 183\ \mu$m].[25]

This paper presents the development of a self-contained acoustic plane wave generator that provides a known sinusoidal shear stress input to a shear-stress sensor. In this calibration technique the sinusoidal shear stress is inferred from the cylindrical Stokes-layer solution for a plane acoustic wave traveling in a circular duct. The theoretical aspects of this technique are discussed and representative calibration results from a floating-element sensor presented.

Background

The dynamic response of a general shear-stress sensor system is band-limited because of the various modes of energy storage and dissipation inherent in the system. Assuming that the shear-stress sensor can be modeled as a linear, time-invariant system over a range of shear stress, dynamic calibration is possible, provided that a known sinusoidal shear input can be produced.[26,27] In this section the theoretical basis for dynamically calibrating linear shear-stress sensors via Stokes-layer excitation in a cylindrical duct is presented.

Stokes-Layer Excitation

The basic principle of this technique relies on the fact that the particle velocity of acoustic waves must equal zero at the duct wall. The consequence of the no-slip boundary condition is the generation of a frequency-dependent boundary layer [$\delta(f)$] and wall shear stress [$\tau(f)$] (Ref. 25) (see Fig. 1). For the case of purely traveling plane waves in a duct with no mean flow, the linearized perturbation equation for the compressible momentum conservation law in the axial direction reduces to the classic problem of a duct-flow driven by an oscillating pressure gradient. The solution to this problem indicates that the magnitude of the shear stress is directly proportional to the product of the pressure magnitude and the square root of the excitation frequency.[25]

The problem of duct flow driven by an oscillating pressure gradient was originally investigated experimentally by Richardson and Tyler,[28] then solved analytically by Sexl.[29] This problem is also discussed in Ref. 25. Assuming an axial velocity $u(r, t)$, where r is the

Presented as Paper 98-0585 at the AIAA 36th Aerospace Sciences Meeting, Reno, NV, 10–11 January 1998; received 6 March 1998; revision received 4 August 2000; accepted for publication 17 August 2000.

*Postdoctoral Associate; currently Assistant Professor, Department of Aerospace Engineering, Mechanics and Engineering Science, University of Florida, Gainesville, FL 32611-6250. Member AIAA.

†Graduate Student; currently Research Scientist, Honeywell Technology Center, 12001 State Highway 55, Plymouth, MN 55441.

‡Professor, Microsystems Technology Laboratories, 39-567-B.

§Assistant Professor; currently Associate Professor, Division of Engineering, Brown University, Providence, RI 02912-9104. Member AIAA.

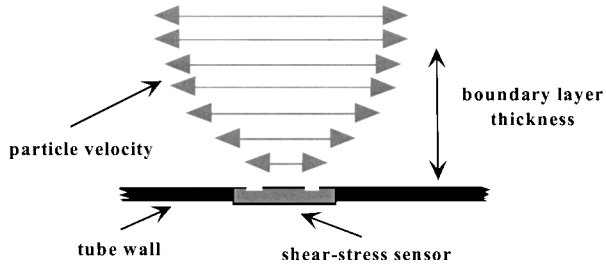

Fig. 1 Schematic of acoustic-wave particle motion near the wall.

radial coordinate, the differential form of the momentum conservation law in the axial direction z is

$$\frac{\partial u}{\partial t} = Ke^{j2\pi ft} + \nu\frac{\partial^2 u}{\partial r^2} + \nu\frac{1}{r}\frac{\partial u}{\partial r} \tag{1}$$

where ρ is the density, ν is the kinematic viscosity, $j = \sqrt{(-1)}$, and $\partial p/\partial z = -\rho Ke^{j2\pi ft}$ is the oscillating pressure gradient. Assuming a harmonic solution, the boundary conditions to the problem consist of a finite velocity at the tube center and the no-slip condition at the tube wall $r = R$,

$$u(0, t) < \infty, \qquad u(R, t) = 0 \tag{2}$$

The solution of Eq. (1) for the particle velocity $u(r, t)$ is

$$u(r, t) = \frac{Ke^{j2\pi ft}}{j2\pi f}\left[1 - \frac{I_0(r\sqrt{j2\pi f/\nu})}{I_0(R\sqrt{j2\pi f/\nu})}\right] \tag{3}$$

where I_0 is the zeroth-order, modified Bessel function[30] and μ is the fluid viscosity. The corresponding wall shear stress induced by the oscillating pressure gradient is

$$\tau(2\pi f, t) = \frac{-Ke^{j2\pi ft}}{j2\pi f}\sqrt{j2\pi f\rho\mu}\frac{I_1(R\sqrt{j2\pi f/\nu})}{I_0(R\sqrt{j2\pi f/\nu})} \tag{4}$$

If the oscillating pressure gradient is driven by a plane, purely traveling (in positive z direction only), acoustic wave

$$p = p' \exp[j(2\pi ft - kz)] \tag{5}$$

then the pressure gradient can be expressed as

$$e^{j2\pi ft}\frac{\partial p}{\partial z} = \frac{-j2\pi f}{c}p' \exp[j(2\pi ft - kz)] \tag{6}$$

where p' is the magnitude of the pressure fluctuation, c is the speed of sound, and $k = 2\pi f/c$ is the axial wave number. Combining Eqs. (3), (4), and (6) results in the particle velocity and wall shear stress generated by a purely traveling acoustic wave in a circular duct:

$$u(r, z, t) = \frac{p' \exp[j(2\pi ft - kz)]}{\rho c}\left[1 - \frac{I_0(r\sqrt{j2\pi f/\nu})}{I_0(R\sqrt{j2\pi f/\nu})}\right] \tag{7}$$

$$\tau(z, t) = -\frac{p' \exp[j(2\pi ft - kz)]}{c}\sqrt{\frac{j2\pi f\mu}{\rho}}\frac{I_1(R\sqrt{j2\pi f/\nu})}{I_0(R\sqrt{j2\pi f/\nu})} \tag{8}$$

Equation (8) indicates that the magnitude of the oscillating shear stress is directly proportional to the product of the acoustic pressure magnitude and the square root of the excitation frequency.

The validity of this solution will break down at higher frequencies, where the assumption of plane-wave propagation is no longer valid. In addition to the plane wave propagating in axial direction possessing uniform transverse wave fronts, there are higher-order wave modes that reflect back and forth from the duct walls.[31] Therefore, the frequency bandwidth over which the preceding solution is valid is dependent on the acoustic wave-guide characteristics of the tube.

Plane-Wave Propagation in a Tube

The propagation of higher-order modes in a cylindrical duct with zero mean flow is governed by the wave equation for simple harmonic waves[31]

$$\nabla^2 p' + (2\pi f/c)^2 p' = 0 \tag{9}$$

For a circular duct of radius R, the eigenfunctions in cylindrical coordinates are

$$p_{mn}(r, \phi, z, t) = p' \exp[j(2\pi ft \pm k_{mn}z)]\begin{matrix}\cos(m\phi)\\ \sin(m\phi)\end{matrix} J_m(\pi q_{mn}r/R) \tag{10}$$

where J_m is the Bessel function of order m[30] and q_{mn}/R is the corresponding eigenvalue. If the walls of the tube are assumed to be rigid, the resulting eigenvalue problem is

$$J'_m(\pi q_{mn}) = 0 \tag{11}$$

where the prime denotes differentiation with respect to the radial coordinate. The (m, n)th mode has m plane modal surfaces that extend radially outward from center axis and n cylindrical nodes that are concentric about the axis. The corresponding wave number is

$$k_{mn} = \sqrt{(2\pi f/c)^2 - (\pi q_{mn}/R)^2} \tag{12}$$

When k_{mn} is real, Eq. (10) represents traveling waves, axially propagating in the positive z direction. If k_{mn} is imaginary, then the mode is evanescent, exponentially decaying as it propagates in the positive z direction. The fundamental mode (0, 0) has a zero characteristic value and is thus a plane wave. The first higher-order mode that becomes propagational (nonevanescent) is the (1, 0) mode or first "spinning" mode. The characteristic value associated with (1, 0) is $q_{10} = 0.5861$, and the corresponding frequency is[31]

$$f_{co} = 0.2931c/R \tag{13}$$

This value represents the upper limit or cutoff frequency for the validity for Eq. (8) in a tube of radius R. For example, the cutoff frequency for a 0.5-m -radius tube is approximately 200 Hz.

Experimental Apparatus

The experimental study was performed in the Fluid Dynamics Research Laboratory at the Massachusetts Institute of Technology. A plane-wave tube capable of generating purely traveling, plane acoustic waves was designed and fabricated. Two series of tests were conducted: one to characterize the response of the plane-wave tube and the other to demonstrate the Stokes-layer dynamic calibration technique by calibrating a floating-element shear-stress sensor.

Plane-Wave Tube

The experimental apparatus used to generate the oscillating Stokes layer, a plane-wave tube, is shown in Fig. 2. The setup includes a 6 ft-long, 2 in.-diam, $\frac{1}{8}$ in.-thick, circular acrylic tube with a speaker driver (JBL 2446J) (Ref. 32) attached at one opening and

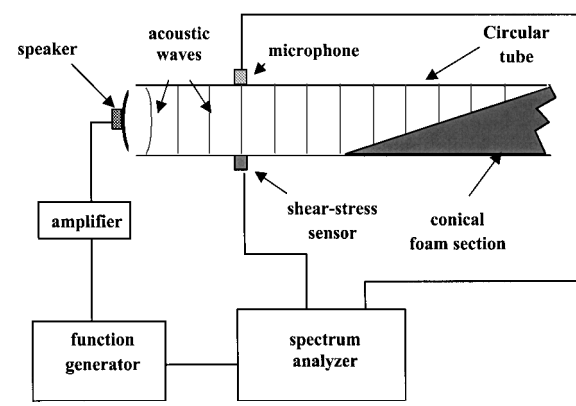

Fig. 2 Schematic of plane-wave tube apparatus used for generating an oscillating shear stress.

a conical foam section (HyFonic, 80 ppi; Stephenson & Lawyer, Inc.) filling the other end. A Stanford Research Systems SR 830 Lock-In Amplifier provided a sinusoidal input to a Crown DC-300A Series II amplifier, which in turn drove the speaker. The conical foam section prevented acoustic reflections by dissipating the incident traveling waves. A $\frac{1}{8}$-in. microphone (B & K 4138 attached to a B & K 2633 preamplifier) and shear-stress sensor were flush mounted at an axial location 15 in. from the speaker driver, 180 deg opposite one another. The signals from the microphone and shear-stress sensor were recorded by the lock-in amplifier.

As discussed in the preceding section, the wave-guide transmission properties of the circular tube determine the propagation characteristics of the acoustic modes. The bandwidth of the calibrator is thus determined by the low-frequency cutoff of the tube, which is defined by the frequency of the first propagating nonplanar acoustic mode. The low-frequency cutoff for our tube geometry is $\approx$4 kHz [Eq. (13)]. The speaker driver will generate higher-order modes, and so it is important to locate the shear-stress sensor and microphone a distance greater than $\lambda/6(\lambda = c/f)$ downstream of the speaker to ensure measurement of nonevanescent, propagating modes. Proper termination of the plane waves with the foam insert is crucial to prevent wave reflections, which in turn would invalidate the Stokes-layer relationship between pressure and shear stress [Eq. (8)]. Specifically, wave reflections at the tube end will result in a combination of traveling and standing acoustic waves producing nodes and antinodes, as well as a phase shift between the particle velocity and the pressure fluctuation.

Floating-Element Sensor

We have previously reported the detailed design and fabrication of this sensor.[6–9] The sensor is composed of a 500 × 500 μm, square silicon floating element of 7-μm thickness, which is suspended 1 μ above the surface of a silicon wafer by four silicon tethers that are 500 μm long, 7 μm wide, and 7 μm thick (Fig. 3). Photodiodes are integrated into the substrate under the floating element at the leading and trailing edge. A modulated light source (7-mW, 670-nm laser diode) illuminates the element from above such that a differential photocurrent is produced, which is directly proportional to the lateral displacement of the element and hence the shear stress. The photocurrent is converted to voltage via a SR 570 current preamplifier. The photodiode transduction scheme was selected after consideration of a variety of sensing schemes that we have previously implemented.[3–5] This scheme yields a highly sensitive measurement that does not require integration of detection electronics and is substantially insensitive to environmental effects such as electromagnetic interference (EMI) and stray charging when compared with higher-impedance transduction techniques such as capacitive detection.

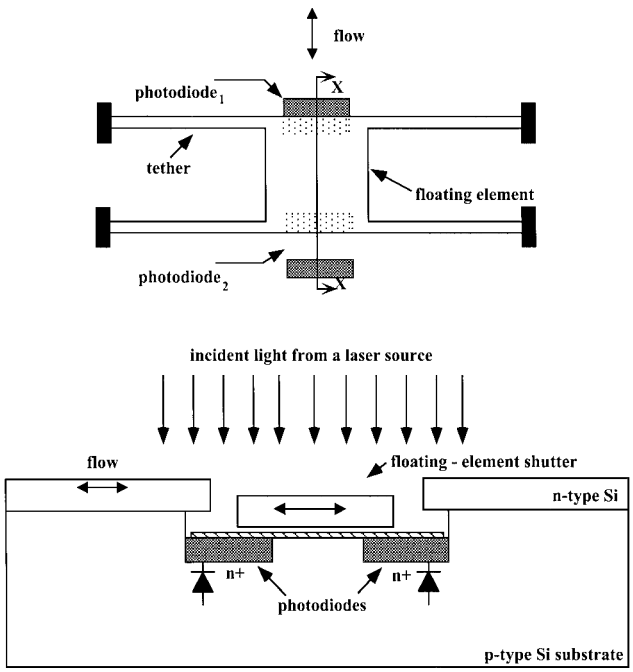

Fig. 3 Schematics of both the top and cross-sectional views of the shear-stress sensor.

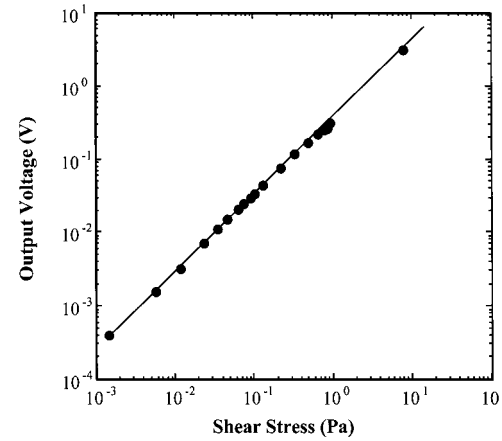

Fig. 4 Static calibration of a 500 × 500 × 7 μm floating-element shear-stress sensor.

As already reported, static calibrations demonstrate the linearity of this device over a shear-stress range of 0.0014–10 Pa (Fig. 4).[9] These data indicate that the sensor responds linearly to within $\pm$1%. In addition, the device has demonstrated minimal drifts in sensitivity.[8] Qualitative spectra from this sensor indicate a bandwidth in excess of 10 kHz.[7] The noise floor of the sensor is 0.0004 Pa. The actual characteristics of the frequency response function, however, are presently unknown. Therefore, in order to use this device to obtain quantitative turbulence information the effects of the inherent mass, compliance, and dissipation of the floating-element structure on the dynamic response must be characterized. In the case of our floating-element sensor, the linearity of the static calibration data and the stability of the system lead to the assumption that the micromachined shear-stress sensor is a linear, time-invariant system. Therefore, the frequency response function $H(f)$ can be obtained by providing the system with a known input and observing the output. In this experiment the known shear-stress $\tau_{St}(f)$ is obtained via Eq. (8), and the measured shear-stress is obtained by dividing the sensor voltage $V(f)$ by the static sensitivity $\partial\bar{V}/\partial\tau$ (Fig. 4):

$$H(f) = \frac{V(f)}{\tau_{St}(f)}\frac{\partial\bar{\tau}}{\partial\bar{V}} \tag{14}$$

Uncertainty Associated with the Dynamic Calibration of Floating-Element Sensors

Ideally, the lateral displacement of the floating element will be solely a function of the applied wall shear stress. In practice, however, it is known that there will be an additional displacement as a result of the pressure gradient forces across the floating element.[8] There are two sources of error caused by the pressure gradient. The first error is associated with net pressure force acting on the lip of the floating element. This force is equal to the product of the differential pressure and the cross-sectional area of the floating element. The second error is caused by the viscous force imposed by flow beneath the floating element. The magnitude of the effective shear stress including pressure-gradient effects for a pressure-driven mean flow in a channel of height h is[8]

$$\tau_{\text{eff}} = (1 + g/h + 2t/h)\tau_{\text{wall}} \tag{15}$$

where t is the lip thickness (7 μm) and g is the depth of the cavity under the element (1 μm). The second and third terms in the bracket of Eq. (15) represent the error caused by flow beneath the element and the net pressure force acting on the lip. Similar forces will act on the tethers of the floating element but will be much smaller because of the reduced pressure gradient over the axial length (7 μm) compared to axial length of the floating element (500 μm). The scaling of these errors clearly points out the advantages of a microfabricated

shear-stress sensor possessing a thin lip and small gap. The mean shear-stress data presented in this paper were taken in a channel of height $h = 508$ μm resulting in a maximum error of 2% (Ref. 8).

There are similar errors induced by the local pressure gradients generated by traveling acoustic waves. The magnitude of the effective shear stress including pressure-gradient effects for a purely traveling acoustic waves in a circular duct is

$$\tau(f)_{\text{eff}} = [1 + (g/2)\sqrt{2\pi f\rho/\mu} + t\sqrt{2\pi f\rho/\mu}]\tau_{\text{wall}} \qquad (16)$$

The second and third terms of Eq. (16) represent the error caused by the fluctuating flow beneath the element and the net fluctuating pressure force acting on the lip (assuming a square element). The magnitude of the error terms is proportional to f, whereas the actual shear stress is proportional to $\sqrt{(f)}$. The error terms are also $\pi/2$ out of phase with the actual shear stress. The fluctuating shear-stress data presented in this paper possessed a maximum error of 3.2 dB at 10 kHz.

Experimental Results

Because the magnitude of the shear stress is proportional to the product of the acoustic pressure and the square root of the excitation frequency [see Eq. (8)], it was necessary to drive the speaker at approximately 150 dB to ensure a measurable signal (e.g., >0.0004 Pa) at the lower frequencies. Figure 5 shows the dynamic response of the Massachusetts Institute of Technology speaker/plane-wave tube system plotted vs the JBL factory specifications.[32] The response monotonically increases from 100 Hz to 1 kHz and then monotonically decreases with increasing frequency. The presence of a notch at 600 Hz corresponds with a resonant structural mode of the acrylic tube. At resonance a portion of the acoustic energy radiated by the speaker drives the structural vibration of the tube rather than propagating downstream. As a result, the microphone measures a lower sound pressure level. After the structural resonance the JBL specifications and our measured results are in agreement to within ± 1 dB up to the cutoff frequency for the (1, 0) mode, $\approx$4 kHz.

The shear-stress sensor output voltage for a sinusoidal pressure sweep at nominally 150 dB is shown in Fig. 6. This represents a fluctuating shear envelope of approximately 0.1 Pa at 100 Hz to 1.0 Pa at 10 kHz. The sensor output exhibits a square-root dependence on frequency as predicted by Eq. (8). It is evident that the sensor is responding to shear stress and not pressure because the square-root frequency dependence dominates the variation in sound-pressure level shown in Fig. 6. The cross-axis sensitivity of the shear-stress sensor to pressure was further tested by rotating the sensor 90 deg to the axial direction. The sensor displayed negligible sensitivity to acoustic forcing at 150 dB. Finally, the voltage output of the sensor displays square-root frequency well beyond the onset of the first higher-order mode. At frequencies greater than 4 kHz, the acoustic field will consist of other modes in addition to the fundamental. Although Eq. (8) is invalid in this region, the sensor appears to be responding to shear stress up to at least 10 kHz.

The magnitude of the normalized, shear-stress sensor frequency-response function [Eq. (14)] is shown in Fig. 7. Ideally, the static and dynamic responses should be equal, resulting in a normalized frequency response function of 0 dB. In Fig. 7 the response is between 0 and 5 dB over the frequency range of 200 Hz to 4 kHz. The positive shift in response is most likely as a result of the Stokes-layer solution underpredicting the actual shear stress caused by the acoustic wave. This underprediction could be associated with tube vibration that would increase the uncertainty in modeling the problem with Eq. (1). In particular, an additional term accounting for the radial wall velocity would be necessary, and a compliant boundary condition would be necessary for the plane-wave eigenvalue problem [Eq. (11)]. In addition, the positive shifts at low frequencies might be caused by reflected waves as a result of ineffective plane-wave tube termination at the longer acoustic wavelengths.

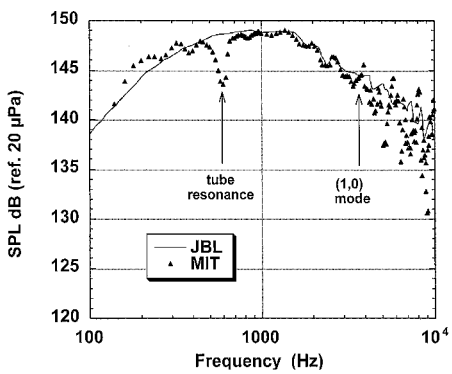

Fig. 5 Plot showing the pressure response of the plane-wave tube and the manufacturers' calibration curve for the JBL 2446J speaker driver.

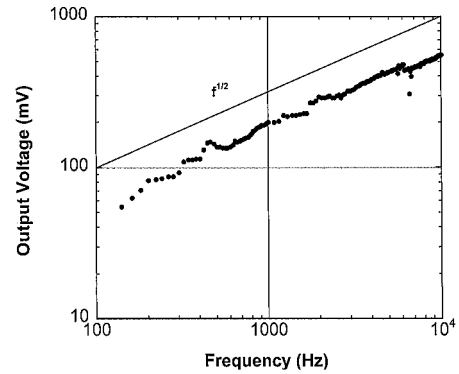

Fig. 6 Output voltage of a 500-μm sensor to acoustic plane-wave excitation.

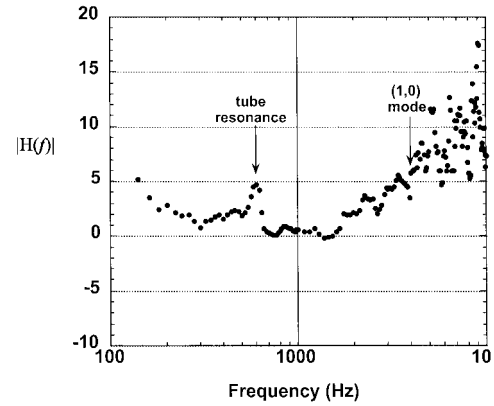

Fig. 7 Bode plot showing the magnitude of the shear-stress sensor frequency response function in decibels as a function of frequency for a 500-μm sensor.

Conclusions

Direct, in situ dynamic calibration of a shear-stress sensor has been achieved. This technique uses plane, purely traveling acoustic waves to generate an oscillating shear stress. The theoretical and practical aspects of this technique are presented. A plane-wave tube apparatus was constructed and a floating-element shear-stress sensor calibrated. According to the theoretical design, the calibration indicates a nominally flat sensor response up 4 kHz, the frequency cutoff of the derived pressure-shear relationship. Based on the square-root frequency scaling of oscillating shear stress, this sensor demonstrates a qualitative response to at least 10 kHz.

Future work in this area will focus on improving the accuracy and bandwidth of the Stokes-layer calibration technique. Specifically, a smaller-area rectangular duct with improved vibration isolation will be investigated. The ultimate goal is to extend this broadband technique to a variable-mean duct flow for the calibration of thermal shear-stress sensors.[5,12–20]

Acknowledgments

Support for this work was provided by the Air Force Office of Scientific Research (Contract F49620-93-1-0194) and NASA (Contract NAG-1-1785). Samples were fabricated and packaged in the

Microsystems Technology Laboratories (MTL), and the staff of the MTL are thanked for their assistance. Silicon-on-insulator wafers for the second-generation sensor fabrication were generously provided by the Motorola Semiconductor Products Sector (Direct Wafer Bonding Group). We would also like to acknowledge Sarah Lee, Mike Fedor, and Chris Protz for their assistance in obtaining the dynamic response data. Finally, the authors thank K. Uno Ingard, Richard Wlezien, and Raimo Hakkinen for their helpful technical discussions.

References

[1]Haritonidis, J. H., "The Measurement of Wall Shear Stress," *Advances in Fluid Mechanics Measurements*, Springer-Verlag, New York, 1989, pp. 229–261.

[2]Breuer, K. S., "Active Control of Wall Pressure Fluctuations in a Turbulent Boundary Layer," Fluid Engineering Div. Vol. 168, American Society of Mechanical Engineers, New York, 1993, pp. 39–48.

[3]Schmidt, M. A., Howe, R. T., Senturia, S. D., and Haritonidis, J. H., "Design and Calibration of a Microfabricated Floating-Element Shear-Stress Sensor," *Transactions of Electron Devices*, Vol. ED-35, 1988, pp. 750–757.

[4]Ng, K., Shajii, J., and Schmidt, M. A., "A Liquid Shear-Stress Sensor Using Wafer-Bonding Technology," *Journal of Microelectromechanical Systems*, Vol. 1, No. 2, 1992, pp. 89–94.

[5]Goldberg, H. D., Breuer, K. S., and Schmidt, M. A., "A Silicon Wafer-Bonding Technology for Microfabricated Shear-Stress Sensors with Backside Contacts," *Proceedings of the Solid-State Sens. Actuator Workshop*, Transducer Research Foundation, Cleveland, OH, 1994, pp. 111–115.

[6]Padmanabhan, A., Goldberg, H. D., Schmidt, M. A., and Breuer, K. S., "A Wafer-Bonded Floating-Element Shear-Stress Microsensor with Optical Position Sensing by Photodiodes," *Journal of Microelectromechanical Systems*, Vol. 5, No. 4, 1996, pp. 307–315.

[7]Padmanabhan, A., Goldberg, H. D., Schmidt, M. A., and Breuer, K. S., "A Silicon Micromachined Sensor for Shear Stress Measurements in Aerodynamic Flows," AIAA Paper 96-0422, Jan. 1996.

[8]Padmanabhan, A., "Silicon Micromachined Sensors and Sensor Arrays for Shear Stress Measurements in Aerodynamic Flows," Ph.D. Dissertation, Dept. of Mechanical Engineering, Massachusetts Inst. of Technology, Cambridge, MA, Feb. 1997.

[9]Padmanabhan, A., Sheplak, M., Breuer, K. S., and Schmidt, M. A., "Micromachined Sensors for Static and Dynamic Shear Stress Measurements in Aerodynamic Flows," *Proceedings of Transducers '97*, Inst. of Electrical and Electronics Engineers, Piscataway, NJ, 1997, pp. 137–140.

[10]Pan, T., Hyman, D., Mehregany, M., Reshotko, E., and Garverick, S., "Microfabricated Shear Stress Sensors, Part 1: Design and Fabrication," *AIAA Journal*, Vol. 37, No.1, 1999, pp. 66–72.

[11]Hyman, D., Pan, T., Reshotko, E., and Mehregany, M., "Microfabricated Shear Stress Sensors, Part 2: Testing and Calibration," *AIAA Journal*, Vol. 37, No.1, 1999, pp. 73–78.

[12]Oudheusden, B., and Huijsing, J., "Integrated Flow Friction Sensor," *Sensors and Actuators A*, Vol. 15, 1988, pp. 135–144.

[13]Liu, C., Tai, Y. C., Huang, J., and Ho, C. M., "Surface Micromachined Thermal Shear Stress Sensor," *Proceedings of the American Society of Mechanical Engineers Symposium on Application of Microfabrication to Fluid Mechanics*, American Society of Mechanical Engineers, New York, 1994, pp. 9–15.

[14]Jiang, F., Tai, Y. C., Gupta, B., Goodman, R., Tung, S., Huang, J. B., and Ho, C. M., "A Surface-Micromachined Shear Stress Imager," *Proceedings of the MEMS '96*, Inst. of Electrical and Electronics Engineers, Piscataway, NJ, 1996, pp. 110–115.

[15]Liu, C., Huang, C.-B., Zhu, Z., Jiang, F., Tung, S., Tai, Y.-C., and Ho, C.-M., "A Micromachined Flow Shear-Stress Sensor Based on Thermal Transfer Principles,"*Journal of Microelectromechanical Systems*, Vol. 8, No. 1, 1999, pp. 90–99.

[16]Kälvesten, E., "Pressure and Wall Shear Stress Sensors for Turbulence Measurements," Ph.D. Dissertation, Dept. of Signals, Sensors and Systems, Royal Inst. of Technology, Stockholm, 1996.

[17]Kälvesten, E., Stemme, G., Vieider, C., and Löfdahl, L., "An Integrated Pressure-Flow Sensor for Correlation Measurements in Turbulent Gas Flows," *Sensors and Actuators A: Physical*, Vol. 52, 1996, pp. 51–58.

[18]Lofdahl, L., Kälvesten, E., Hadzianagnostakis, T., and Stemme, G., "An Integrated Silicon Based Wall Pressure-Shear Stress Sensor for Measurements in Turbulent Flows," *Proceedings of the 1996 American Society of Mechanical Engineers International Mechanical Engineering Congress and Exposition*, American Society of Mechanical Engineers, New York, 1996, pp. 245–251.

[19]Breuer, K. S., "MEMS Sensors for Aerodynamic Applications—the Good, the Bad (and the Ugly)," AIAA Paper 2000-0251, Jan. 2000.

[20]Cain, A., Chandrasekaran, V., Nishida, T., and Sheplak, "Development of a Wafer-Bonded, Silicon Nitride Membrane Thermal Shear-Stress Sensor with Platinum Sensing Element," *Proceedings of the Solid-State Sensor Actuator Workshop*, Transducer Research Foundation, Cleveland, OH, 2000, pp. 300–303.

[21]Jiang, F., Tai, Y. C., Ho, C. M., and Li, W. J., "A Micromachined Polysilicon Hot-Wire Anemometer," *Proceedings of the Solid-State Sensor Actuator Workshop*, Transducer Research Foundation, Cleveland, OH, 1994, pp. 264–267.

[22]Bellhouse, B. J., and Schultz, D. L., "The Determination of Fluctuating Velocity in Air with Thin Film Gauges," *Journal of Fluid Mechanics*, Vol. 29, No. 2, 1967, pp. 289–295.

[23]Brison, J. F., Charnay, G., and Comte-Bellot, G., "Calculation of the Heat Transfer Between a Hot Film and a Substrate Using a Two-Dimensional Model: Prediction of the Dynamic Response for Ordinary Probes," *International Journal of Heat and Mass Transfer*, Vol. 22, No. 1, 1979, pp. 111–119.

[24]Perry, A. E., Smits, A. J., and Chong, M. S., "The Effects of Certain Low Frequency Phenomena on the Calibration of Hot Wires," *Journal of Fluid Mechanics*, Vol. 90, 1979, pp. 415–431.

[25]White, F. M., *Viscous Fluid Flow*, McGraw–Hill, New York, 1974, pp. 143–148.

[26]Oppenheim, A. V., Willsky, A. S., and Young, I. T., *Signals and Systems*, Prentice–Hall, Upper Saddle River, NJ, 1983, Chap. 3.

[27]Bendat, J. S., and Piersol, A. G., *Engineering Applications of Correlation and Spectral Analysis*, Wiley-Interscience, New York, 1993, Chap. 5.

[28]Richardson, E. G., and Tyler, E., "The Transverse Velocity Gradients near Mouths of Pipes in Which an Alternating or Continuous Flow of Air is Established," *Proceedings of the Physical Society of London*, Vol. 42, 1929, pp. 1–15.

[29]Sexl, T. Z., "Über die von E. G. Richardson Entdeckten Annulareffekt," *Physica*, Vol. 61, 1930, pp. 349–362.

[30]Abramowitz, M., and Stegun, I. A., *Handbook of Mathematical Functions*, 9th ed., Dover, New York, 1972, p. 374.

[31]Morse, P. M., and Ingard, K. U., *Theoretical Acoustics*, McGraw–Hill, New York, 1968, Chap. 9.

[32]JBL Professional, 2446H/J Compression Driver Specification Sheet, Northridge, CA, Oct. 1996.

R. P. Lucht
Associate Editor